Shape of precipitates in Ni-Al-Mo single crystals

Jean-Marc Schneider ,[a] Bernd Schönfeld ,[a] Bruno Demé [b] and Gernot Kostorz [a*]

[a]ETH Zürich, Institut für Angewandte Physik, CH-8093 Zürich, Switzerland, and [b]Institut Laue-Langevin, B.P. 156, F-38042 Grenoble, France.
E-mail: kostorz@iap.phys.ethz.ch

A method is presented to determine the shape of the average precipitate from anisotropic small-angle scattering patterns from single crystalline alloys during decomposition. The form factor squared of an average precipitate is described by an analytical expression with a single parameter, the morphology parameter α, to account for changes from spherical to cuboidal shape. The method is applied to microstructural states of Ni-12 at.% Al-2 at.% Mo and Ni-10 at.% Al-5 at.% Mo after aging treatments of up to 10 h at 970 or 1070 K. The value of α increases with aging time and smaller Mo content, in good agreement with the average shape of precipitates obtained from transmission electron microscopy.

1. Introduction

The high mechanical strength of Ni-based superalloys at elevated temperatures is mainly due to the presence of a two-phase microstructure consisting of a fine distribution of hard, coherent γ'-precipitates with the $L1_2$ structure, embedded in the Ni-rich matrix (γ-phase). This compositional heterogeneity and the presence of different crystallographic structures act as an obstacle to the motion of dislocations, giving rise to high strength and creep resistance.

The formation of coherent γ'-precipitates in Ni-Al-Mo has been the subject of many investigations using especially small-angle neutron scattering (SANS) and transmission electron microscopy (TEM) (see, e.g., Calderon *et al.*, 1990; Fährmann *et al.*, 1995; Sequeira *et al.*, 1995). The decomposition kinetics are strongly affected by temperature and composition; increasing the temperature speeds up the decomposition process, while a higher Mo content reduces the rate of decomposition. During the growth of precipitates, strain fields are built up owing to the difference of lattice parameters of the two phases. The lattice mismatch is reduced with increasing Mo content, as Mo primarily increases the lattice parameter of the matrix (Conley *et al.*, 1989). Owing to the elastic strain energy stored in the microstructure, the coarsening process of precipitates is slowed down with increasing lattice mismatch. Furthermore, a change in the shape and arrangement of the precipitates is induced (see, e.g., Fratzl and Paris, 1999, and references therein). Values characterizing the microstructure, like the morphology of precipitates, their size distribution and spatial arrangement are accessible using TEM. However, a large number of micrographs is required to achieve a sufficient accuracy for quantitative results. Besides, the spatial resolution may become a limiting factor when early stages of decomposition are investigated. As another tool, SANS has been successfully employed in the investigation of decomposed Ni-based alloys (see, e.g., Kostorz, 1996).

The aim of the present investigation is the quantitative analysis of the microstructure, especially concerning the shape of the precipitates, as a function of composition and heat treatment. Reliable data for a description of decomposition in the presence of coherency strains are thus provided.

2. Experimental

High-purity nickel (99.99 at.%, Materials Research, Germany), aluminum (99.999 at.%, VAW Aluminium, Germany) and molybdenum (99.95 at.%, Materials Research, Germany) were melted together in an alumina crucible under argon atmosphere in an induction furnace. The melt was poured into a copper mould to produce cylindrical ingots of alloys with the nominal composition Ni-12 at.% Al-2 at.% Mo and Ni-10 at.% Al-5 at.% Mo. Rods with a diameter of 10 mm were used to grow single crystals by the Bridgman technique. Discs, 3.5 mm in thickness, were cut by spark erosion with surfaces parallel to {110} planes. They were mechanically polished (final polish with 6 μm diamond spray). After homogenization at 1270 K for 24 h, they were rapidly brought to the aging temperature of 970 or 1070 K, kept within the quenching furnace for 1, 3 or 10 h, and rapidly quenched to room temperature in chilled water. The final composition of the alloys was controlled by X-ray fluorescence analysis using a Ni-8 at.% Al-8 at.% Mo single crystal as standard. Relative differences in the Al and Mo content for alloys with the same nominal composition were smaller than ±0.2 atomic percent.

Samples intended for TEM investigations were cut from single-crystalline rods grown under the same nominal conditions. Small discs, 3 mm in diameter and 0.3 mm in thickness, were cut by spark erosion. They were electrochemically thinned until perforation, using an electrolyte composed of 400 ml methanol, 40 ml butyloxyethanol, 14.4 ml nitric acid (65%) and 1.5 ml perchloric acid (70%). The electrolyte was cooled at 218 K.

The SANS measurements were performed at room temperature in vacuum on the D11 instrument at ILL (Grenoble, France). Samples were measured with detector distances of 1.1, 5 and 20 m. The collimation distance was set to 5.5 m for the first two configurations and to 20.5 m for the latter. The wavelength of the incident neutrons was 0.6 nm, the wavelength spread $\Delta\lambda/\lambda = 10\,\%$ (FWHM). Scattering patterns were corrected for parasitic scattering and converted to macroscopic differential cross-sections by calibrating with the scattering of water. As the sample environment was chosen without any window close to the sample, the signal-to-noise ratio was larger than 250 at any detector pixel for all configurations.

3. Data evaluation and microstructure modeling

Generally, evaluation of SANS intensities may be classified into the so-called model-free methods and those based on a model that compare an assumed microstructure to the measured intensity distribution. For particulate systems consisting of two phases, various model-free methods are available. These are Guinier's procedure for the determination of the radius of gyration giving a typical size of precipitates, the determination of Porod's invariant accounting for the volume fraction of the precipitates, Porod's law allowing the total interfacial area to be determined, and the

Figure 1
Dark-field transmission electron micrograph of a Ni-12 at.% Al-2 at.% Mo alloy after aging at 1070 K for 10 h.

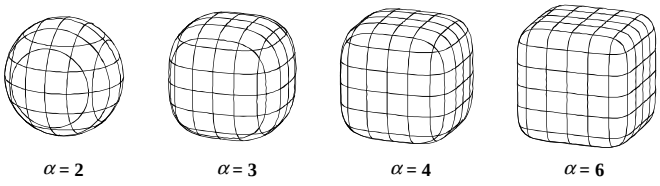

Figure 2
Schematic view of precipitate boundaries as defined by Eq. (1) for various values of the morphology parameter α and constant half-lengths R.

calculation method of the correlation function between phases after Bueche & Debye. These methods, however, are most suitable for statistically isotropic systems and do not fully exploit the information from anisotropic SANS data. Hence, additional information is usually required to determine physically or geometrically relevant quantities.

For the data treatment presented here, a simple expression is proposed to describe the shape of precipitates (Figs. 1 and 2). The vectors of the precipitate boundary, with components *x*, *y*, *z* in a three-dimensional Cartesian system, satisfy the equation

$$|x|^{\alpha} + |y|^{\alpha} + |z|^{\alpha} = R^{\alpha}, \qquad (1)$$

where R denotes the half-length size of the precipitate along the *x*, *y* and *z*-axes, and α is the morphology parameter. This analytical expression was chosen because it only requires a single parameter, the morphology parameter α, to account for the observed changes in the shape of precipitates from a sphere ($\alpha = 2$) to a cube (α tending to infinity).

The form factor is evaluated for each morphology by means of a numerical Fourier transformation of the precipitate volume, defined on a three-dimensional cubic grid containing 8×10^6 to 10^9 points. For efficient calculation, the form factor is only calculated for directions corresponding to experimental data. The Fourier transform is split into a two-dimensional sum over vectors perpendicular to the direction of the scattering vector and a one-dimensional Fourier transform of this projection. The effects of a finite wavelength spread and a particle size distribution are taken into account by smearing the form factor squared in radial direction using a Gaussian size distribution $w(R)$ according to

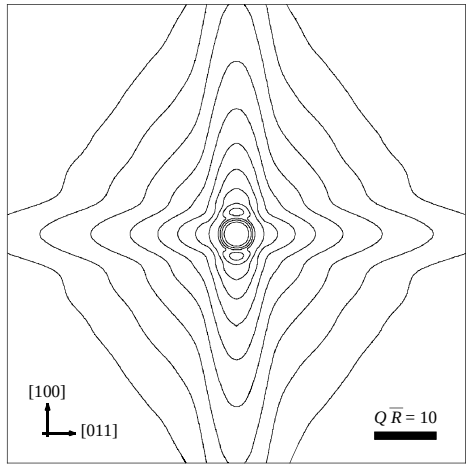

(*a*)

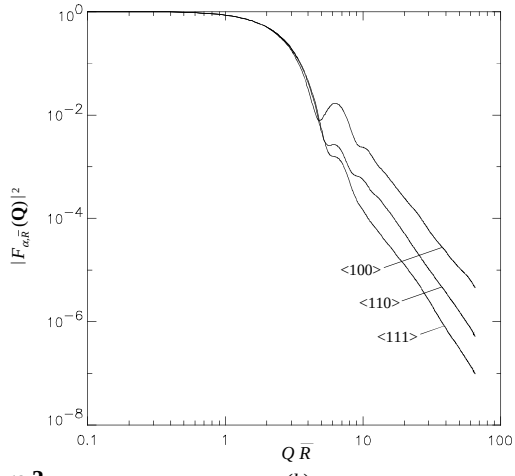

(*b*)

Figure 3
Form factor squared $|F_{\alpha,\overline{R}}(\mathbf{Q})|^2$ for an ensemble of precipitates with morphology parameter $\alpha = 3$. The precipitate sizes are normally distributed with a standard deviation of 5%. The axes are scaled with respect to the size $\overline{R}$ of the representative precipitate [calculated according to Eq. (3)]: (*a*) within a $(01\bar{1})$ plane with lines of equal intensities separated by a factor of $\sqrt{10}$; (*b*) along the mean crystallographic directions <100>, <110> and <111>.

$$\left|F_{\alpha,\overline{R}}(\mathbf{Q})\right|^2 = \frac{\int \left|F_{\alpha}(\mathbf{Q},R)\right|^2 v_{\alpha}{}^2 R^6 \, w(R)\,dR}{\int v_{\alpha}{}^2 R^6 \, w(R)\,dR}, \qquad (2)$$

where $\mathbf{Q}$ denotes the scattering vector of modulus $Q = 4\pi \sin\theta/\lambda$ (with λ = wavelength and θ = half the scattering angle), $F_{\alpha}(\mathbf{Q},R)$ is the form factor of a precipitate with half-length R along the *x*, *y* and *z*-axes and morphology parameter α, v_{α} is the proportionality factor between the volume of the precipitate and R^3, and $F_{\alpha,\overline{R}}(\mathbf{Q})$ is the form factor of the ensemble (Fig. 3). The size of the average precipitate, $\overline{R}$, that is representative for the scattering of the ensemble, is determined as

$$\overline{R}^6 = \frac{\int R^6 \, w(R)\,\mathrm{d}R}{\int w(R)\,\mathrm{d}R}. \qquad (3)$$

After calculation of the squared form factors over a range of morphology parameters up to $\alpha = 8$, the coordinate systems of the model and the measurement are scaled using the average particle size $\overline{R}$. The value of $\overline{R}$ is taken from the 6th moment of the particle size distribution as determined by an analysis of TEM micrographs. The morphology parameter is determined by matching the intensity profiles along the crystallographic directions <100> and <110> at large scattering vectors ($Q\overline{R} > 4\pi$). The scattering intensity at large scattering vectors depends most predominantly on the shape of precipitates as scattering effects of correlations in precipitate arrangement become negligible.

4. Results and discussion

The scattering patterns of both alloys after aging at 970 and 1070 K for 3 h are shown in Fig. 4. As a common feature, a high anisotropy in scattering is observed over the whole range of magnitude in scattering vectors. This anisotropy is due to the non-spherical shape of the precipitates and to the high correlation in their spatial arrangement. Systematic differences among the various scattering patterns can nevertheless be seen. For example, the scattering of the Ni-12 at.% Al-2 at.% Mo (Figs. 4*c*, *d*) shows a larger anisotropy than observed for the Ni-10 at.% Al-5 at.% Mo (Figs. 4*a*, *b*). Furthermore, an increase in anisotropy with increasing aging temperature is observed in both cases. The morphology parameter is determined from the ratio between scattering intensities along the crystallographic axes <100> and <110> for scattering vectors between 0.4 and 0.8 nm^{-1}, a range that is not much affected by interparticle interference effects and still provides sufficient counting rates. As the scattering intensity has nearly the same power-law behavior for large values of the scattering vector (where the fitting is performed), a high precision in the value of the morphology parameter is achieved. Especially, its value does not depend much on the value of the average size. The fitting curves are in good agreement with the experimental data in the fitting range (Fig. 5). At smaller scattering vectors, a comparison between experimental and model curves is not useful, since the effects of particle interference are not included in the model. Even at large scattering vectors the whole two-dimensional patterns are in general not perfectly reproduced, especially along the <111> directions. This deficiency seems to be related to local deviations from cubic symmetry in the shape of the precipitates; adding an aspect ratio as an additional degree of freedom is expected to remove this discrepancy.

Results of the morphology parameter and the intensity prefactor for the different samples are summarized in Table 1. This intensity prefactor corresponds to the value (independent of scattering vector) of the scattering cross-section divided by the average form factor squared. It consists of the product of the scattering contrast $(\Delta\rho)^2$, the number of precipitates per unit volume, and their mean volume squared. During the later stages of decomposition this prefactor must increase (see Table 1).

To check the relevance of the presented method, these results were compared with the shape of precipitates from TEM observations. Precipitates seen in dark-field electron micrographs were analyzed

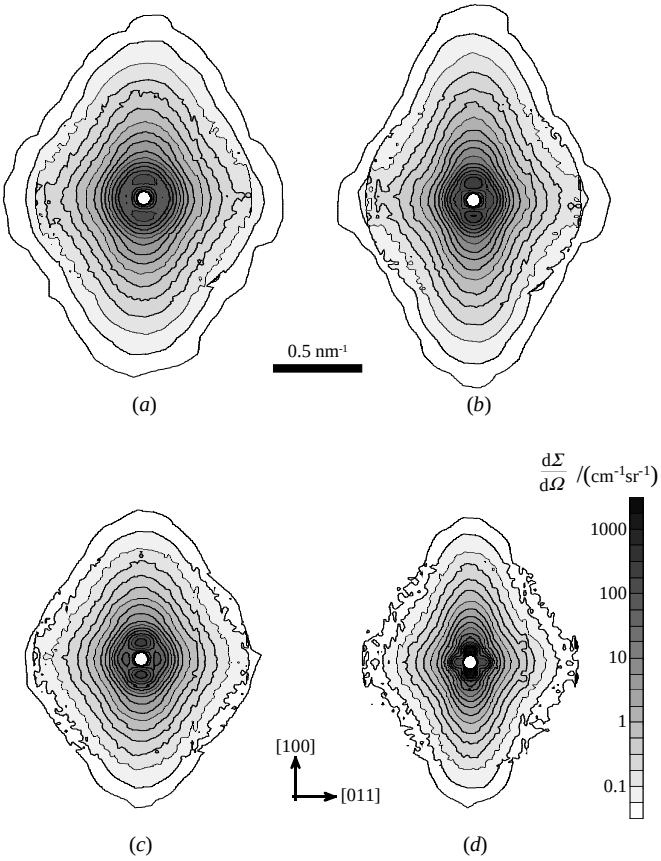

Figure 4
Experimental macroscopic scattering cross-sections $d\Sigma/d\Omega$ of (*a*,*b*) Ni-10 at.% Al-5 at.% Mo and (*c*,*d*) Ni-12 at.% Al-2 at.% Mo single crystals after aging for 3 h at 970 (*a*,*c*) and 1070 K (*b*,*d*).

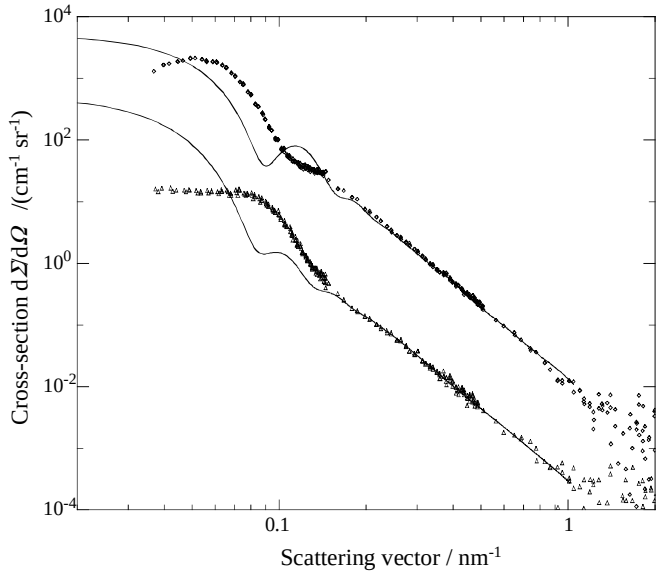

Figure 5
Experimental cross-sections along <100> (diamonds) and <110> (triangles) for a Ni-10 at.% Al-5 at.% Mo single crystal after aging at 1070 K for 10 h. The curves representing the best fit (solid lines) were calculated with a morphology parameter $\alpha = 2.94$. Intensities along the <110> direction are divided by a factor of 10 for clarity.

Table 1
Morphology parameter and intensity prefactor for the different states. The intensity factor times the form factor describes the total macroscopic cross-section in the region of large scattering vectors.

Alloy composition	Heat treatment	Morphology parameter α	Intensity prefactor (10^6 cm^{-1} sr^{-1})
Ni-12 at.% Al-2 at.% Mo	970 K / 1 h	2.89	172
Ni-12 at.% Al-2 at.% Mo	970 K / 3 h	3.03	204
Ni-12 at.% Al-2 at.% Mo	970 K / 10 h	3.11	286
Ni-12 at.% Al-2 at.% Mo	1070 K / 1 h	2.95	415
Ni-12 at.% Al-2 at.% Mo	1070 K / 3 h	3.18	5742
Ni-12 at.% Al-2 at.% Mo	1070 K / 10 h	3.79	9468
Ni-10 at.% Al-5 at.% Mo	970 K / 1h	2.53	131
Ni-10 at.% Al-5 at.% Mo	970 K / 3 h	2.68	161
Ni-10 at.% Al-5 at.% Mo	970 K / 10 h	2.89	191
Ni-10 at.% Al-5 at.% Mo	1070 K / 1 h	2.50	71.5
Ni-10 at.% Al-5 at.% Mo	1070 K / 3 h	2.65	138
Ni-10 at.% Al-5 at.% Mo	1070 K / 10 h	2.94	954

using quantitative image analysis procedures to obtain precipitate sizes and the location of each precipitate center. These data were used to build a two-valued image $I_{\rm bw}$ for the spatial distribution of the γ- and the γ'-phase. The correlation function $I(\mathbf{x})$, which is the conditional probability of finding the γ'-phase at $\mathbf{x}$ if a precipitate is centered at the origin, is calculated according to

$$I(\mathbf{x}) = \frac{\sum_i R_i^6 \, I_{bw}(\mathbf{x} - \mathbf{x}_i)}{\sum_i R_i^6} \quad , \qquad (4)$$

where $\mathbf{x}$ is the location of any image pixel, $\mathbf{x}_i$ and R_i denote the location and the size of the precipitate i; an example is shown in Fig.6. From the two-dimensional correlation function, the average precipitate interface is obtained as the line of steepest decrease in the conditional probability. Its shape is in good agreement with the result from model fitting (shown as a dark line in Fig.6). However, taking systematic errors into account, the absolute error in the determination of the morphology parameter is estimated to be ±0.2.

5. Conclusion

The method presented here is suitable for the evaluation of anisotropic scattering patterns from single crystalline alloys and provides an average parameter for the shape of the precipitates. Despite the difficulties in restoring the maximum informational content from two-dimensional scattering patterns with respect to the average shape of the precipitates, the proposed method seems to describe a characteristic feature of particles in a real microstructure rather well. Especially, it was shown that the fitted shape and the average shape from TEM micrographs are in good agreement. Furthermore, the method appears to be more sensitive than TEM owing to the large number of precipitates analyzed by SANS.

Using this method, characteristic features of a microstructure can be conveniently followed during the decomposition process, which is a prerequisite for the understanding of the microscopic phenomena governing decomposition and coarsening of alloys under the influence of coherency strains.

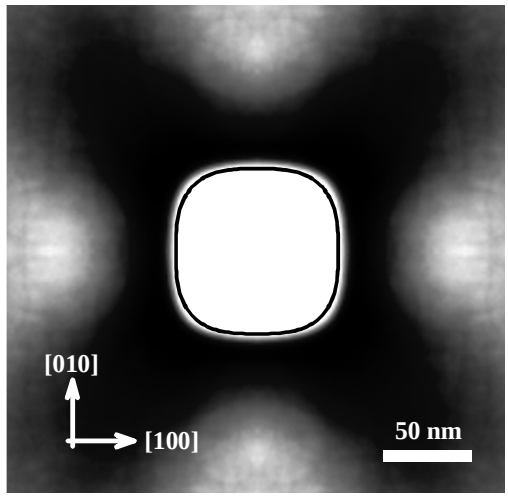

Figure 6
Conditional probability of finding the γ'-phase if the center of a precipitate is at the center of the figure (probability = 1: white, = 0: black). Data are taken from a dark-field micrograph of a Ni-12 at.% Al-2 at.% Mo alloy after aging at 1070 K for 10 h. Pixels of medium gray level in the inner part of the figure describe the boundary of the average precipitate. The black line close to it represents the boundary of the average precipitate calculated with the morphology parameter $\alpha = 2.94$ and a size reduced by 4% from the value of $\overline{R}$.

The authors are grateful to E. Fischer for growing the single crystals and to S. Ciccariello for fruitful discussions. This work was supported in part by the Swiss National Science Foundation.

References

Calderon, H.A., & Kostorz, G. (1990). *Morris E. Fine Symposium*, edited by P.K. Liaw, H.L. Marcus, J.R. Weertman & J.S. Santner, pp. 11-16. Warrendale, Pa.: The Minerals, Metals and Materials Society.

Conley, J.G., Fine, M.E. & Weertman, J.R. (1989). *Acta Metall.* **37**, 1251-1263.

Fährmann, M., Fratzl, P., Paris, O., Fährmann, E. & Johnson, W.C. (1995). *Acta Metall. Mater.* **43**, 1007-1022.

Fratzl, P. & Paris, O. (1999). *Phase Transitions* **67**, 707-724.

Kostorz, G. (1996). *X-ray and Neutron Scattering*, in *Physical Metallurgy*, 4th edition, edited by R.W. Cahn & P. Haasen, pp. 1115-1199. Amsterdam: North-Holland.

Sequeira, A.D., Calderon, H.A., Kostorz, G. & Pedersen, J.S. (1995). *Acta Metall. Mater.* **43**, 3427-3439; *ibid.* **43**, 3441-3451.